Proceedings of the ASME 2010 3rd Joint US-European Fluids Engineering Summer Meeting and 8th International Conference on Nanochannels, Microchannels, and Minichannels
FEDSM-ICNMM2010
August 1-5, 2010, Montreal, Canada

FEDSM-ICNMM2010-31001

DESIGN OF VOLUMETRIC SOLAR FLOW RECEIVERS

Ananthanarayanan Veeraragavan
Postdoctoral Associate,
Device Research Laboratory,
Department of Mechanical Engineering,
Massachusetts Institute of Technology
Cambridge, MA, USA

Andrej Lenert
Graduate Student,
Device Research Laboratory
Department of Mechanical Engineering
Massachusetts Institute of Technology
Cambridge, MA, USA

Salem Al-Dini
Assistant Professor,
Mechanical Engineering Dept,
King Fahd University of Petroleum and Minerals
Box 5069 Dhahran 31261,
Saudi Arabia

Evelyn N. Wang
Assistant Professor, Device Research Laboratory
Department of Mechanical Engineering
Massachusetts Institute of Technology
Cambridge, MA, USA

ABSTRACT

The development of efficient solar thermal receivers has received significant interest for thermal energy to electrical power conversion and heating applications. Volumetric receivers, where the incoming solar radiation is absorbed in a fluid volume, have advantages over state-of-the-art surface absorbers owing to the reduced heat losses at the surface. To efficiently distribute and store the thermal energy in the volume, nanoparticles can be suspended in the liquid medium to scatter and absorb the incoming radiation. In such systems, however, compact models are needed to design and optimize the performance. In this paper, we present an analytical model that can be used to perform parametric studies to investigate the effect of heat loss, particle distribution, and flow rate on receiver efficiency. The analytical model was formulated by modeling the suspended nanoparticles as embedded heat sources. The heat equation was solved with the surface heat losses modeled using convective losses based on *Newton's* law of cooling. The analytical solution provides a convenient tool to predict two-dimensional temperature profiles for a variety of heat loss and inlet fluid temperature conditions. The efficiency of the receiver is defined as the ratio of the amount of thermal energy transported by the fluid to the total incident solar energy. For very large lengths the thermal energy carried by the fluid reaches a maximum steady value as the amount of heat loss equals the incident solar energy. The model can be used to estimate the approximate receiver lengths required to achieve near peak bulk fluid temperature. The results from this study will help guide experimental design, as well as practical flow receivers for solar thermal systems. Predictions made on a channel of 1mm depth with a solar concentration of 1 show that there exists a maximum system efficiency of 0.3373 for a dimensionless receiver length of 1.66.

INTRODUCTION

Most solar thermal technologies today, ranging from hot water heating to concentrated solar power, use absorbing surfaces to convert energy from its radiative form into thermal energy. Black surfaces and selective surfaces are very efficient at performing this type of conversion, but they are not very well suited for transferring heat to a carrier fluid. Direct absorption of solar radiation inside the fluid medium promises to be a more efficient heat transfer mechanism.

In the case of conversion of thermal to electrical power, solar thermal power plants aim to operate at higher temperatures. As the temperature of the receiver surface increases, the corresponding losses to the environment begin to contribute significantly to the loss in the overall conversion efficiency of solar energy.

Small, absorbing particles suspended inside a heat transfer fluid have been proposed by Abdelrahman [1] and Hunt [2] in order to minimize the temperature difference between the absorber and the carrier fluid. The temperature difference between the absorbing particles and the fluid is negligible owing to the particles' large surface to volume ratio [2, 3]. To model the coupled radiative and convective heat transfer inside

the particle-based receivers, researchers have developed numerical models capable of predicting the response of these systems at high temperatures. Kumar and Tien [4] investigated a flowing molten salt receiver seeded with small particles, while Miller has modeled solar absorption inside a rectangular receiver and oxidation of carbon particles using a three-dimensional model [3, 5]. Experimental work by Drotning determined the optical properties of such molten salt suspensions [6]. More recently, Phelan *et al.* have made recent contributions in numerical modeling of nanoparticles [7], and measurement of optical properties of candidate transparent fluids for this application [8].

Despite the previous modeling efforts, an analytical model describing volumetric receivers does not exist. Even for relatively simple geometries of volumetric receivers, numerous parameters can be varied and it becomes difficult to predict the outcome of the coupled radiative and heat transfer equations. Consequently, current models require implementing relatively complicated and slow numerical schemes. An analytical model gives a solar thermal engineer a quick tool to predict the outcome of varying parameters such as particle loading and concentration, in order to assess the viability of a volumetric receiver design for the application. Volumetric absorbers promise to be more efficient than surface absorbers, but predicting this increased efficiency can be complicated. The objective of this study is to present an analytical method to describe volumetric solar thermal receivers for temperatures below (800 K) which can be used as a starting point for more complicated models and designs.

NOMENCLATURE

C	Solar concentration factor [-]
C_p	Heat capacity [J/kg-K]
f_v	Particle volume fraction [-]
G	Green's functions
G_s	Incident solar radiation [W/m^2]
H	Receiver height [m]
I	Radiative intensity [W/m^2-μm]
L	Length of Receiver [m]
c	Speed of light [m/s]
h	Planck's Constant [J-s]
k	Thermal conductivity [W/m-K]
m	Complex refractive index [-]
n	Index of refraction [-]
q	heat release [W/m^3]
T	Temperature [K]
U	Plug-flow velocity [m/s]
x, y	Coordinates [m]

Greek Symbols

β	Extinction coefficient [1/m]
η	Efficiency [-]
θ	Dimensionless temperature change [-]
κ	Absorptive index [-]
λ	Wavelength [m]
ρ	Density [kg/m^3]
σ	Stefan-Boltzmann constant [W/m-K^4]

Superscript

$\bar{}$	Dimensionless quantity
$\dot{}$	Time derivative
$'''$	Per unit volume [m^{-3}]

Subscripts

abs	Absorbed
f	Fluid medium
in	Receiver inlet
λ	Spectral
p	Particle
rec	Receiver
s	Solar

MODEL FORMULATION

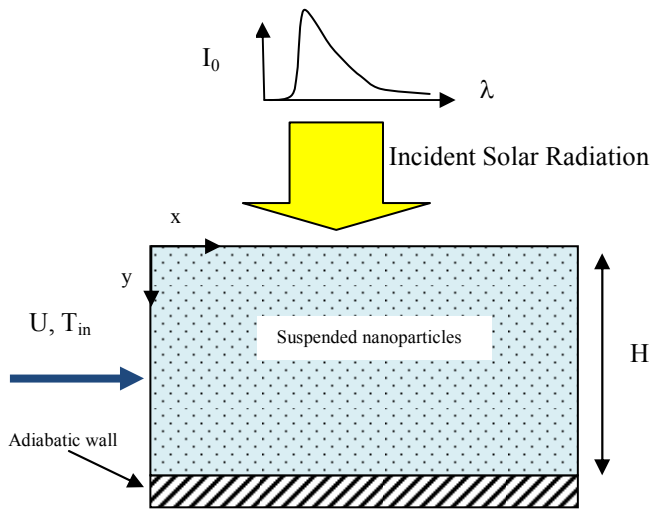

Figure 1. Schematic of the volumetric solar flow receiver with suspended nanoparticles.

Figure 1 shows the schematic of the volumetric solar receiver. The solar receiver is a parallel plate channel of height *H*. The fluid with the suspended nanoparticles enters from the left and the channel is exposed to solar radiation from the top. The energy equation for the receiver shown in Fig. 1 accounting for the volumetric heat release (owing to the presence of the suspended nanoparticles) can be written as

$$\rho U C_p \frac{\partial T}{\partial x} = k \frac{\partial^2 T}{\partial y^2} + \dot{q}'''(y) \tag{1}$$

The boundary conditions are

$$\left.\frac{\partial T}{\partial y}\right|_{y=H} = 0 \tag{2a}$$

$$k\left.\frac{\partial T}{\partial y}\right|_{y=0} = h_E\,(T_{y=0} - T_{amb}) \tag{2b}$$

$$T\big|_{x=0} = T_{in} \tag{2c}$$

Equation 2a arises from the assumption of an adiabatic bottom surface, while Eq. 2b is due to heat loss at the top surface modeled by *Newton's* law of cooling with a heat loss coefficient (h_E). Eq. 2c is set by the fluid entering the receiver with a uniform inlet temperature (T_{in}). The energy equation and the boundary conditions are cast in a non-dimensional form using the following dimensionless parameters

$$\bar{y} = \frac{y}{H}; \quad \bar{x} = \frac{x}{H} \tag{3}$$

$$\theta = \frac{k\left(T - T_{in}\right)}{C\,G_s\,H} \tag{4}$$

$$\overline{\dot{q}'''}(\bar{y}) = \frac{\dot{q}'''(y)\,H}{C\,G_s} \tag{5}$$

Equation 2 gives the dimensionless spatial coordinates; non-dimensionalized using the channel height (H). θ is the dimensionless temperature; non-dimensionalized using the fluid thermal conductivity (k), incident solar flux (G_s = 1000 W/m^3) and concentration (C)

$$Pe\frac{\partial\theta}{\partial\bar{x}} = \frac{\partial^2\theta}{\partial\bar{y}^2} + \overline{\dot{q}'''}(\bar{y}) \tag{6}$$

The corresponding boundary conditions are

$$\left.\frac{\partial\theta}{\partial\bar{y}}\right|_{\bar{y}=1} = 0 \tag{7a}$$

$$\left.\frac{\partial\theta}{\partial\bar{y}}\right|_{\bar{y}=0} = Nu_E\,(\theta_{\bar{y}=0} - \theta_{amb}) \tag{7b}$$

$$\theta\big|_{\bar{x}=0} = 0 \tag{7c}$$

The non-dimensional *Peclet* and heat loss *Nusselt* numbers are defined below

$$Pe = Re\,Pr = \frac{\rho U C_p H}{k} \tag{8}$$

$$Nu_E = \frac{h_E H}{k} \tag{9}$$

The difference between the fluid inlet temperature and the ambient temperature is captured by θ_{amb} defined as

$$\theta_{amb} = \frac{k\left(T_{amb} - T_{in}\right)}{C\,G_s\,H} \tag{10}$$

ANALYTICAL SOLUTION

Equation 6 can be solved by a combined homogeneous and particular integral solution for a known volumetric heat release profile (see Appendix A for details). The solution can be expressed as

$$\begin{aligned}\theta &= \theta_{\text{hom}} + \theta_{PI} \\ &= \sum_{n=1}^{\infty} A_n e^{-\lambda_n^2\,\bar{x}} Y_n\left(\bar{y}\right) \;+\; \int_0^1 G(\bar{y},\xi)\,\overline{\dot{q}'''}(\xi)\,d\xi\end{aligned} \tag{11}$$

The volumetric heat release function (in the dimensional form) is determined by an energy balance assuming that change in the spectrally integrated radiation intensity (I), due to attenuation by the medium, is dissipated as a local heat release. Thus, the heat release profile is

$$\dot{q}'''(y) = -\frac{d}{dy}\int_0^{\infty} I_\lambda\left(y\right)d\lambda \tag{12}$$

Planck's expression (Eq. 13) for black body radiation at an estimated Sun's temperature (T_{sun} = 5800 K) is

$$I_{Planck}\left(\lambda, T_{sun}\right) = \frac{2hc^2}{\lambda^5}\frac{1}{e^{hc/\lambda k_B T_{sun}} - 1} \tag{13}$$

This is weighted by a constant (S_C) that accounts for the distance of the earth's surface from the sun

$$S_C = \frac{G_s}{\int_0^{\infty} I_{Planck}\left(\lambda, T_{sun}\right)d\lambda} \tag{14}$$

and supplied as the concentrated (C), incident solar intensity ($I_{0,\lambda}$) entering the flow receiver at the top surface

$$I_{0,\lambda} = C\,S_C\,I_{Planck}\left(\lambda, T_{sun}\right) \tag{15}$$

For wavelengths of incident solar radiation, the spectral radiative transfer equation (RTE) for attenuation of light in the y-direction (Fig. 1) is

$$\frac{dI_\lambda}{dy} = -(\beta_{f,\lambda} + \beta_{p,\lambda}) I_\lambda \tag{16}$$

where, β_f and β_p are the extinction coefficients of the fluid and particles respectively. In general, the spectral absorption coefficient for pure fluids is related to the index of absorption (κ_f) by the equation [9]

$$\beta_{f,\lambda} = \frac{4\pi\kappa_f}{\lambda} \tag{17}$$

Similarly, in the limit of low volume fraction ($f_v << 0.01$), and small particle size diameter, the particle extinction coefficient is given by the expression [9, 10]

$$\beta_{p,\lambda} = \frac{6\pi k_1 f_v}{\lambda} \tag{18}$$

Where, k_1 is defined as in Eq. 19 and m is the ratio of complex refractive index of the particles divided by the real part of the refractive index of the medium [9, 11]

$$k_1 = Im\left\{\frac{m^2 - 1}{m^2 + 2}\right\}; \quad m = \frac{n_p + i\kappa_p}{n_f} \tag{19}$$

Equation 16 can be solved to give I as a function of y

$$I_\lambda(y) = I_{0,\lambda}\, e^{-(\beta_{f,\lambda}+\beta_{p,\lambda})y} \tag{20}$$

Assuming that the optical properties (m) of the fluid and particles are spectrally independent, the spectral power density at a given depth (y) can be obtained by integrating Eq. 21 over all wavelengths as given below

$$P(y) = \int_0^\infty I_\lambda(y)\, d\lambda = \frac{15 C G_s}{\pi^4}\phi_3\left(1 + \frac{2k_B(3f_v k_1 + 2k_f)\pi T_{sun}\, y}{hc}\right) \tag{21}$$

where, $\phi_n(x)$ is the *PolyGamma* function of order n. Equation 21 is used in Eq. 12 to finally obtain the heat release profile as

$$\dot{q}'''(y) = -\frac{30 C G_s\, k_B\, T_{sun}(3f_v k_1 + 2k_f)}{hc\pi^3}\phi_4\left(1 + \frac{2k_B(3f_v k_1 + 2k_f)\pi T_{sun}\, y}{hc}\right) \tag{22}$$

Equation 22 is a complex expression involving the optical properties of the fluid and particles. However, once the material choices are made for the fluid and the particle, the only unknown is the volume fraction. Eq. 22 is substituted in Eq. 5 to obtain the non-dimensional heat release profile as

$$\overline{\dot{q}'''}(\bar{y}) = -\frac{30 k_B\, T_{sun}(3f_v k_1 + 2k_f)H}{hc\pi^3}\phi_4\left(1 + \frac{2k_B(3f_v k_1 + 2k_f)\pi T_{sun}\, H\, \bar{y}}{hc}\right) \tag{23}$$

Equation 23 shows that the non-dimensional heat release profile depends on f_v and H.

MODEL RESULTS

The analytical model is used to predict the influence of the various control parameters on the performance of the volumetric solar receiver. From the problem formulation and resulting solution it is clear, that for a given type of fluid and particle, the parameters that influence the solution are: C, f_v, H, Pe, Nu_E. In the following subsections the influence of these different parameters is explored.

Heat release profiles:

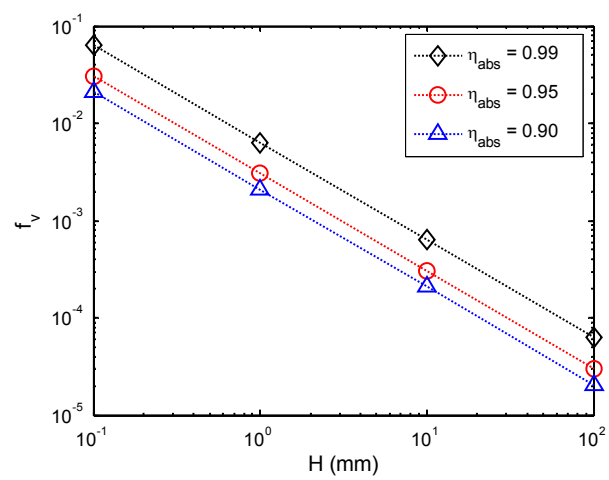

Figure 2. Particle volume fraction as a function of channel height for different η_{abs}.

It was shown in Eq. 23 that the non-dimensional heat release profile depends on f_v and H. It can be noted from Eq. 18 that for the light intensity to be zero at the bottom surface of the receiver, the particle extinction coefficient and hence f_v would have to be infinite. In practical receivers, it would be required that the bulk of the incident radiative flux is been absorbed and released as heat. In order to perform meaningful calculations using the analytical solution, it becomes necessary to specify what portion of the incident light is absorbed before it reaches the bottom surface. This fraction is defined as

$$\eta_{abs} = 1 - \frac{P(H)}{P(0)} \tag{24}$$

Once η_{abs} is chosen and H is fixed, Eqs. 21 and 24 can be used to calculate the f_v required. Figure 2 shows a log-log plot of f_v

as a function of H for different η_{abs}. The figure shows that as the channel height decreases the particle volume fraction required to guarantee a certain absorption fraction increases. In this paper we study a mini channel (H = 1mm with solar concentration = 1) assuming an attenuation value of $\eta_{abs} = 0.99$. The choice of these two parameters fixes f_v required as 0.006344, for Therminol-VP1 (n_f = 1.63, κ_f = 3.86 e-8 at λ_{peak} = 0.5 μm) with suspended carbon nanoparticles (n_p = 2.72, κ_p = 0.2 at λ_{peak} = 0.5 μm) [8, 12, 13]. The value of f_v is in the range of validity (f_v << 0.01) for the assumption made for the particle's extinction coefficient. After calculating f_v, Eq. 23 can be used to estimate the heat release function. The resulting profile is shown in Figure 3.

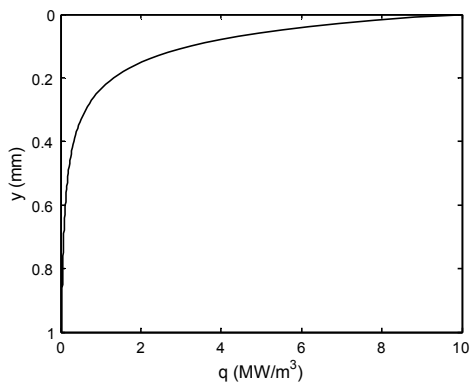

Figure 3. Volumetric heat release function (H = 1mm, η_{abs} = 0.99).

Temperature Profiles:

Figure 4 shows the 2-D non-dimensional temperature profile in the channel for Nu_E = 1, Pe = 5, θ_{amb} = 0. It can be seen that θ increases as x/H increases and approaches a constant value for large x/H. Figure 5 shows the transverse temperature profiles for the same operating conditions as in Fig. 4 for different axial locations. Close to the inlet the top surface temperature is higher than the bottom surface, but this trend reverses far away from the inlet. Figure 6 shows the axial temperature profiles at the top and bottom surface along with the average temperature profile. The top surface temperature drops (owing to heat loss) at large x/H, demonstrating that the volumetric receiver performs as expected, i.e. keeping the surface temperature lower than the bulk temperature. The reason for the average temperature to be greater than the top and bottom temperatures at large x/H is because the temperature peak occurs in between the top and bottom surface (as seen in Fig. 5)

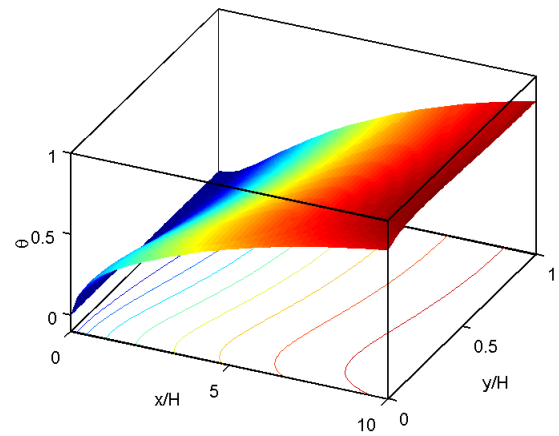

Figure 4. Generalized volumetric receiver model with plug-flow and heat generation (Nu_E = 1, Pe = 5).

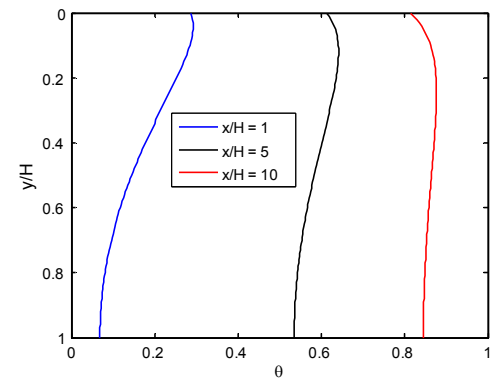

Figure 5. Transverse non-dimensional temperature profiles at different axial locations (Nu_E = 1, Pe = 5).

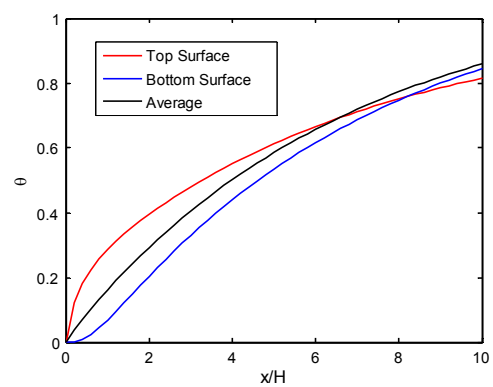

Figure 6. Axial non-dimensional top surface, bottom surface and average temperature profiles (Nu_E = 1, Pe = 5).

Performance and Design:

The temperature profiles shown in Figs. 4-6 enhance the qualitative understanding of the performance of the volumetric receiver and confirm the physically intuitive trends that are expected. For large values of x/H the non-dimensional

temperature reaches a steady value. This is because the surface temperature reaches a high enough value and therefore the heat losses through the surface equal the incoming solar power. This can be expressed as

$$k\left.\frac{\partial T}{\partial y}\right|_{y=0} = h_E\,(T_{y=0} - T_{amb})_{x=\infty} = CG_s \qquad (25)$$

In the non-dimensional space this becomes

$$\left.\frac{\partial \theta}{\partial \bar{y}}\right|_{\bar{y}=0} = Nu_E\,(\theta_{\bar{y}=0} - \theta_{amb})_{\bar{x}=\infty} = 1$$
$$\theta(\infty)_{\bar{y}=0} = \frac{1}{Nu_E} + \theta_{amb} \qquad (26)$$

Eq. 26 shows that for large x/H the non-dimensional surface temperature only depends on the heat loss *Nusselt* number. Corresponding to this condition the bulk fluid also reaches a maximum steady temperature given by

$$\bar{\theta}_{\max} = \bar{\theta}(\infty) = \int_0^1 \theta(\infty, \bar{y})d\bar{y} \qquad (27)$$

In theory an infinitely long receiver is required to realize this maximum temperature. However, in practical devices we would want to limit the length of the receiver. Using the model we can calculate the length required to reach a certain fraction ($\eta_{\Delta T}$) of the maximum temperature given by

$$f_{\theta,\max} = \frac{\bar{\theta}}{\bar{\theta}_{\max}} \qquad (28)$$

Figure 7 shows the non-dimensional length of the receiver ($L^*_{Rec} = L_{Rec}$/H) required to reach the average fluid temperature specified by $f_{\theta,max}$ for two different *Pe* numbers. The figure shows that for a smaller *Pe* number this length is shorter. When the fluid and particle type is fixed, the *Pe* is a measure of the flow rate. When the height of the channel is also fixed, the *Pe* is a direct measure of the flow speed. For lower *Pe*, the flow speed is lesser and hence the residence time of the fluid medium in the channel is more and therefore it reaches the same temperature over a shorter length as compared to a higher *Pe* case. The efficiency of the receiver (η_{Rec}) can be defined as

$$\eta_{Rec} = \frac{(\rho U H)C_p(\bar{T} - T_{in})}{C\,G_s L_{Rec}} = \frac{Pe\,\bar{\theta}(L^*_{\mathrm{Re}\,c})}{L^*_{\mathrm{Re}\,c}} \qquad (29)$$

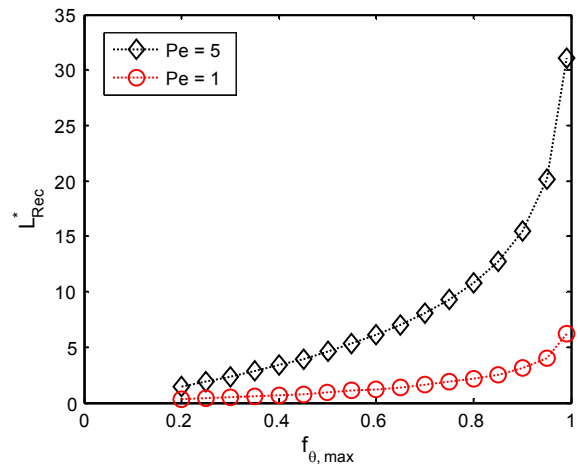

Figure 7. Length of the receiver as a function of fraction of maximum non-dimensional temperature.

Figure 8 shows the variation of η_{Rec} with $f_{\theta,max}$ for two different *Pe* numbers. As expected, the overall efficiency does not depend on the *Pe*.

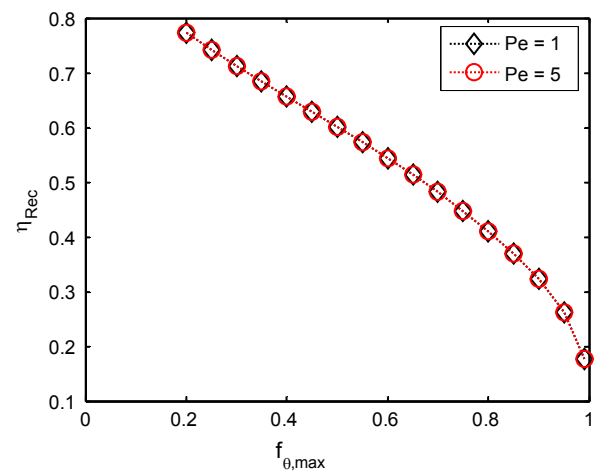

Figure 8. Receiver efficiency vs. fraction of maximum non-dimensional bulk temperature for two *Pe* numbers (Nu_E = 1).

The overall efficiency decreases as the temperature fraction increases and becomes zero for a temperature fraction value of 1 owing to the infinite receiver length required to realize this value. More importantly, the figure shows that fairly realistic temperature fractions (~0.8) can be realized with an overall efficiency around 0.4. Therefore, as the length of the receiver is shortened the ΔT that can be realized is smaller; however, overall receiver efficiency will be higher.

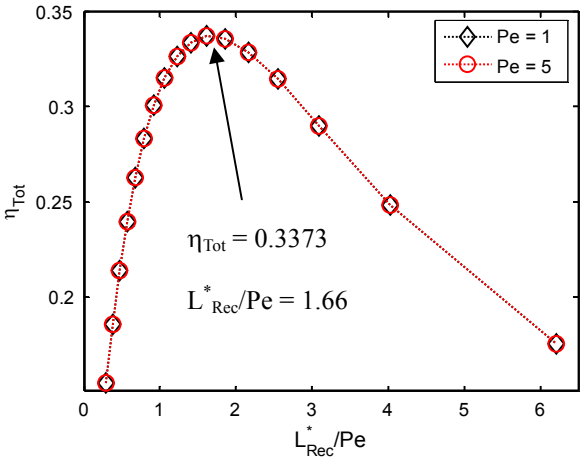

Figure 9. Total efficiency for power generating system as a function of the ratio of the non-dimensional receiver length to *Pe* number (Nu_E = 1, H = 1mm).

In power generation applications where the volumetric solar receiver will be coupled to a power generation cycle, the total efficiency for the system will be a product of the efficiency of the receiver multiplied by the efficiency of the power generation system. For the present study, we can describe an effective total efficiency that accounts for the net effect of the receiver efficiency and the total ΔT produced as

$$\eta_{tot} = \eta_{Rec} f_{\theta,\max} \tag{30}$$

Figure 9 plots the η_{tot} as a function of the ratio of the non-dimensional receiver length to the *Pe* number. Remarkably, the curves for two different *Pe* number collapse on top of each other proving that the total efficiency is independent of the *Pe* number when the channel height is fixed. In other words, the maximum total efficiency is independent of the velocity of the flow. Further, it can be calculated using the analytical mode that the total efficiency has a peak of 0.3373 at $L^*_{Rec}/Pe = 1.6618$.

CONCLUSIONS

Volumetric flow receivers with dispersed nanoparticles were studied for solar-thermal applications. An analytical model was developed in order to study their performance and explore the effect of the different governing parameters and thereby aid in design. Channels of 1mm depth were studied by imposing 99% absorption of solar radiation in one pass (from top surface to bottom). Temperature profiles showed that the top surface temperature is greater than the bottom wall temperature close to the inlet but this trend reverses at locations far away from the inlet showing that the bulk of the fluid (with the embedded nanoparticles) was absorbing the radiation as heat. The model also showed that the maximum ΔT that can be obtained in the receiver depends only on the surface heat loss *Nusselt* number and did not depend on the *Peclet* number. Increasing the *Pe* number increased the distance over which the specified ΔT is reached indicating that it would be better to design volumetric receivers of shorter length with lower flow rates. The model was used to demonstrate that there is a trade-off between the receiver's overall efficiency and the maximum ΔT achieved. Finally, for power generation cycles using a volumetric solar receivers it was shown that there exists a maximum system efficiency of 0.3373 for a dimensionless receiver length of 1.66.

ACKNOWLEDGMENTS

The authors would like to thank the King Fahd University of Petroleum and Minerals in Dhahran, Saudi Arabia, for funding the research reported in this paper through the Center for Clean Water and Clean Energy at MIT and KFUPM.

REFERENCES

1. Abdelrahman, M., P. Fumeaux, and P. Suter, *Study Of Solid-Gas-Suspensions Used For Direct Absorption Of Concentrated Solar-Radiation.* Solar Energy, 1979. **22**(1): p. 45-48.
2. Hunt, A.J., *Small Particle Heat Exhangers*. 1978, Lawrence Berkeley Laboratory.
3. Miller, F.J. and R.W. Koenigsdorff, *Thermal modeling of a small-particle solar central receiver.* Journal Of Solar Energy Engineering-Transactions Of The Asme, 2000. **122**(1): p. 23-29.
4. Kumar, S. and C.L. Tien, *Analysis of Combined Radiation and Convection in a Particulate-Laden Liquid-Film.* Journal of Solar Energy Engineering-Transactions of the Asme, 1990. **112**(4): p. 293-300.
5. Miller, F. and R. Koenigsdorff, *Theoretical-Analysis Of A High-Temperature Small-Particle Solar Receiver.* Solar Energy Materials, 1991. **24**(1-4): p. 210-221.
6. Drotning, W.D., *Optical-Properties of Solar-Absorbing Oxide Particles Suspended in a Molten-Salt Heat-Transfer Fluid.* Solar Energy, 1978. **20**(4): p. 313-319.
7. Tyagi, H., P. Phelan, and R. Prasher, *Predicted Efficiency of a Low-Temperature Nanofluid-Based Direct Absorption Solar Collector.* Journal Of Solar Energy Engineering-Transactions Of The Asme, 2009. **131**(4).
8. Otanicar, T.P., P.E. Phelan, and J.S. Golden, *Optical properties of liquids for direct absorption solar thermal energy systems.* Solar Energy, 2009.
9. Modest, M.F., *Radiative Properties of Particulate Media*, in *Radiative Heat Transfer (Second Edition)*. 2003, Academic Press: Burlington. p. 361.
10. Brewster, M.Q. and C.L. Tien, *Radiative Transfer in Packed Fluidized Beds: Dependent Versus Independent Scattering.* Journal of Heat Transfer, 1982. **104**(4): p. 573-579.
11. Bohren, C.F. and D.R. Huffman, *Absorption and scattering of light by small particles*. Wiley Professional pbk. ed. 1998, New York: Wiley-VCH. xiv, 530 p.

12. Brewster, M.Q., *Thermal Radiative Transfer and Properties*. 1992, NY: John Wiley & Sons.
13. Palik, E.D., *Handbook of Optical Constants of Solids*. 1998: Elsevier.

APPENDIX A

DERIVATION OF THE ANALYTICAL SOLUTION

The methodology adopted is to split the solution into two parts 1) A homogeneous part (without the source term) and 2) A particular integral which accounts for the source term

$$\theta(\bar{x},\bar{y}) = \theta_{\text{hom}}(\bar{x},\bar{y}) + \theta_{PI}(\bar{y}) \tag{A-1}$$

Homogenous part:
The homogenous part of the solution satisfies the following equation and boundary conditions

$$Pe\frac{\partial\theta_{\text{hom}}}{\partial\bar{x}} = \frac{\partial^2\theta_{\text{hom}}}{\partial\bar{y}^2} \tag{A-2}$$

$$\left.\frac{\partial\theta_{\text{hom}}}{\partial\bar{y}}\right|_{\bar{y}=1} = 0 \tag{A-3a}$$

$$\left.\frac{\partial\theta_{\text{hom}}}{\partial\bar{y}}\right|_{\bar{y}=0} = Nu_E\ \theta_{\text{hom},\bar{y}=0} \tag{A-3b}$$

Notice that the homogeneous part of the solution has no source terms and has only linear boundary conditions. The solution to Eq. A-2 is sought using separation of variables in the two dimensions. This yields a solution as

$$\theta_{\text{hom}} = \sum_{n=1}^{\infty} A_n e^{-\lambda_n^2\bar{x}} Y_n(\bar{y}) \tag{A-4}$$

Where the eigenfunctions (Y_n) are given by,

$$Y_n(\bar{y}) = \frac{Cos(\sqrt{Pe}\lambda_n(\bar{y}-1))}{Sin(\sqrt{Pe}\lambda_n)} \tag{A-5}$$

The λ_n's are the eigenvalues for this problem obtained when we attempt to satisfy (after separation of variables) the boundary condition at the top surface of the receiver (Eq. A-3b). The equation for this is as given below

$$Y_n'(0) = Nu_E \cdot Y_n(0) \tag{A-6}$$

The method to get an analytical expression for the coefficients in Eq. A-4 (A_n's) will be described later.

Particular Integral:
We seek a particular integral that satisfies

$$\frac{\partial^2\theta_{PI}}{\partial\bar{y}^2} + \overline{q'''}(\bar{y}) = 0 \tag{A-7}$$

The particular integral is constructed using *Green's* functions (G). This involves viewing the contribution of an elemental source and obtaining the temperature field due to the elemental source and then integrating over the entire space to get the contributions due to the distributed source (i.e., using the principle of superposition). Let the source be located at $\bar{y} = \xi$, then the *Green's* function is required to satisfy the following equation and boundary conditions

$$G''(\xi,\bar{y}) = -\delta(\bar{y}-\xi) \tag{A-8}$$

$$G'\big|_{\bar{y}=1} = 0 \quad and \quad G'\big|_{\bar{y}=0} = Nu_E\left(G\big|_{\bar{y}=0} - Z\right) \tag{A-9}$$

The unknown constant Z will be determined from the boundary condition (eq. 6b) to be satisfied for θ at $\bar{y} = 0$. The construction of the *Green's* function is done as follows. First we recognize from the governing equation for the *Green's* function (eq. 14) that the following jump conditions hold true. These are obtained by requiring continuity of G and by integrating Eq. A-8 across a small control volume near $\bar{y} = \xi$.

$$G\big|_{\bar{y}=\xi^-} = G\big|_{\bar{y}=\xi^+} \quad and \quad G'\big|_{\bar{y}=\xi^+} - G'\big|_{\bar{y}=\xi^-} = -1 \tag{A-10}$$

And because of the definition of δ function at $\bar{y} \neq \xi$ we have

$$G''(\xi,\bar{y}) = 0 \tag{A-11}$$

Solving Eq. A-11 in the two regions where $\bar{y} \neq \xi$ leads to a solution of the Green's function as

$$G(\xi,\bar{y}) = \begin{cases} C\bar{y} + D; & \bar{y} \le \xi \\ E\bar{y} + F; & \bar{y} \ge \xi \end{cases} \tag{A-12}$$

C, D, E and *F* can be solved for by subjecting Eq. A-12 to the boundary conditions (Eq. A-9) and the jump conditions (Eq. A-10). This finally gives the *Green's* function as

$$G(\xi,\bar{y}) = \begin{cases} \dfrac{1}{Nu_E} + \bar{y} + Z; & \bar{y} \le \xi \\ \dfrac{1}{Nu_E} + \xi + Z; & \bar{y} \ge \xi \end{cases} \tag{A-13}$$

Using *Green's* function the particular integral solution is written as

$$\theta_{PI} = \int_0^1 G(\bar{y},\xi)\, \overline{\dot{q}'''}(\xi) d\xi \tag{A-14}$$

Therefore, the final solution can then be written out as

$$\begin{aligned} \theta &= \theta_{\text{hom}} + \theta_{PI} \\ &= \sum_{n=1}^{\infty} A_n e^{-\lambda_n^2 \bar{x}} Y_n(\bar{y}) \quad + \quad \int_0^1 G(\bar{y},\xi)\, \overline{\dot{q}'''}(\xi) d\xi \end{aligned} \tag{A-15}$$

Requiring θ satisfy the boundary condition at the top surface (Eq. 7b) gives

$$Z = \frac{\theta_{amb}}{\int_0^1 \overline{\dot{q}'''}(\xi) d\xi} \tag{A-16}$$

Evaluation of Coefficients:

The only remaining unknowns in Eq. A-15 are the A_n's. To compute the A_n's we require Eq. A-15 to satisfy Eq. 7c (inlet boundary condition). This gives

$$\sum_{n=1}^{\infty} A_n Y_n(\bar{y}) \quad + \quad \int_0^1 G(\bar{y},\xi)\, \overline{\dot{q}'''}(\xi) d\xi \quad = \quad 0 \tag{A-17}$$

Y_n's form an orthogonal basis as the ODE for Y fits the Sturm-Liouville set of equations. Therefore, performing $\int_0^1 (Eq.A-17) \times Y_m(\bar{y}) d\bar{y}$ and rearranging gives

$$A_m = \frac{-\int_0^1 \left(\int_0^1 G(\bar{y},\xi)\, \overline{\dot{q}'''}(\xi) d\xi \right) Y_m(\bar{y}) d\bar{y}}{\int_0^1 Y_m^2(\bar{y}) d\bar{y}} \tag{A-18}$$

Using Eq. A-18 to express A_n's in Eq. A-15 gives the final solution.